Electronic Supplementary Information

Efficient Alkaline Water Electrolysis with Iron-Incorporated Yttrium Oxide/Yttrium Phosphide Nanorods Catalyst on Ni foam: Overpotential Reduction and Electrochemical Insights

Subash Pandey and Rudy Luck*

Department of Chemistry, Michigan Technological University, 1400 Townsend Drive, Houghton, MI 49931

Houghton, MI 49931

*Corresponding author

Contents

1. Experimental

1.1 Chemicals

All the chemicals were used as procured. Yttrium (III) chloride hexahydrate ($YCl_3.6H_2O$, 99.9% trace metal basis), polyvinylpyrrolidone ($(C_6H_9NO)_n$), urea($(CH_4N_2O$, 99.0-100.5%), iron(III) chloride, anhydrous ($FeCl_3$, ≥99.9% trace metal basis), potassium hydroxide (KOH pellets, ≥85%), and platinum on 5 wt.% activated carbon (Pt-C) was obtained from Sigma Aldrich. Sodium hydroxide (NaOH, 98%) from Fisher Scientific, 5% Nafion solution from Ion Power, and Ethanol 200 Proof were procured from Decon Labs, Inc. The Ni foam of 110PPI was procured from MSE Supplies®. All the solutions were prepared in nanopure water (18.2 MΩ cm, Millipore Inc.).

1.2 Electrochemical Characterizations

The electrochemical measurements were performed in a 1 M KOH solution (pH~14). The potential measured using the Ag/AgCl reference electrode was converted to the reversible hydrogen electrode using Nernst's equation,

$$E_{RHE} = E_{Ag/AgCl} + 0.059 \times pH + 0.197\ V$$

$$E_{RHE} = E_{Ag/AgCl} + 1.023\ V$$

100% iR correction was done by the on-the-fly correction method to correct voltage loss between a working electrode and a reference electrode caused by the electrolytic solution.[1] Also, the overpotential after 100% iR compensated and uncompensated is compared.

$$E_{corrected} = E_{measured} - iR_{solution}$$

The Tafel slope was calculated from the linear portion of semi-logarithmic Tafel's plots using the Tafel equation,[2] $\eta = a + b \log j$, where, η, b, and j are overpotential, Tafel slope, and current density, respectively. The term a is related to the exchange current density (j_o) as, a = -Tafel slope × $\log(j_o)$

The electrochemically active surface area (ECSA) was measured by performing cyclic voltammetry (CV) in a non-Faradic region at 10 different scan rates (10, 20, 30, 40, 50, 60, 70, 80,

90, and 100 mVsec-1) in a 1M KOH solution under a nitrogen atmosphere. The working voltage for the OER was set between 1.323 and 1.423 V vs. RHE, and for the HER, it was between 1.223 and 1.224 V vs. RHE. Before the CV scans, a 100% iR compensation was applied. A platinum electrode was used as the counter electrode and an Ag/AgCl electrode was used as the reference electrode. ECSA was calculated as, ECSA= C_{dl}/Cs, where C_{dl} is the double-layer capacitance which is proportional to the ECSA value. The value of Cdl is calculated as, $C_{dl} = \Delta j/2v$, where Δj is the difference between anodic and cathodic current density, and v is the scan rate of CV.

Time-based coulometry measurements were performed for the stability test.

Two electrode measurements were performed using FeYP11 as both cathode and anode for overall water-splitting performance. The Faradic efficiency was determined by dividing moles of hydrogen gas generated by theoretically calculated value from electrolysis.

The electrochemical mechanism for water splitting reaction in alkaline solution was supposed to occur through the following ways,

OER (Adsorbate evolution mechanism [3]):

$OH^- + A \rightarrow A\text{-}OH^* + e^-$ ΔG_1

$A\text{-}OH^* + OH^- \rightarrow A\text{-}O^* + H_2O + e^-$ ΔG_2

$A\text{-}O^* + OH^- \rightarrow A\text{-}OOH^* + e^-$ ΔG_3

$A\text{-}OOH^* + OH^- \rightarrow A + O_2 + H_2O + e^-$ ΔG_4

HER [2]:

$H_2O + e^- \rightarrow OH^- + A\text{-}H^*$ Volmer step (ΔG_a)

$A\text{-}H^* + A\text{-}H^* \rightarrow H_2$ Tafel step (ΔG_a)

$A\text{-}H^* + e^- + H_2O \rightarrow H_2 + OH^-$ Heyrovsky step (ΔG_a)

where * denotes adsorption on surface active sites (A) of the active material.

2. Results

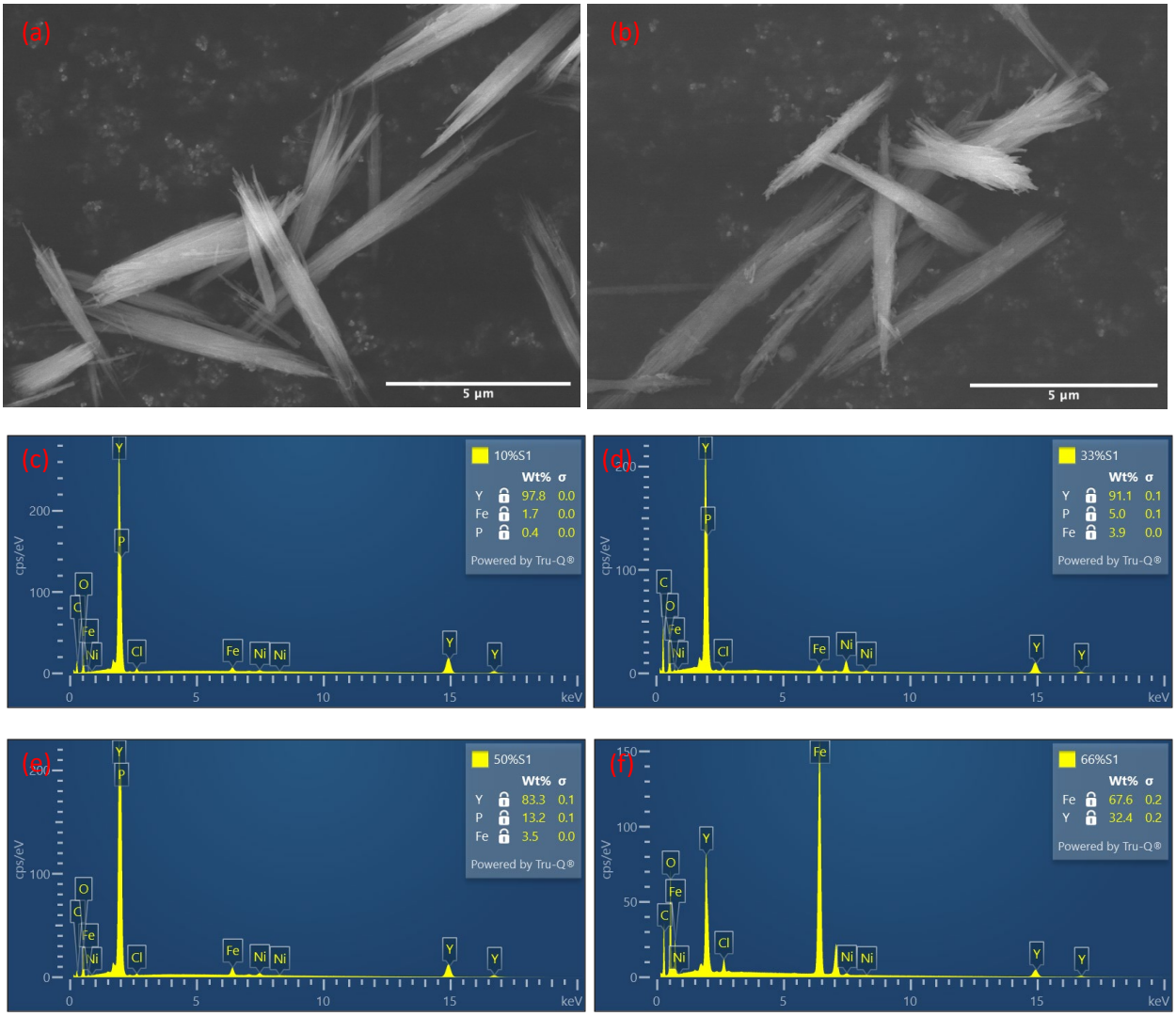

Figure S1: SEM images of (a) Y_2O_3 nanoparticles, and (b) FeYO11, and EDX spectra of (a) FeYP19, (b) FeYP12, (c) FeYP11, and (d) Fe-YP21.

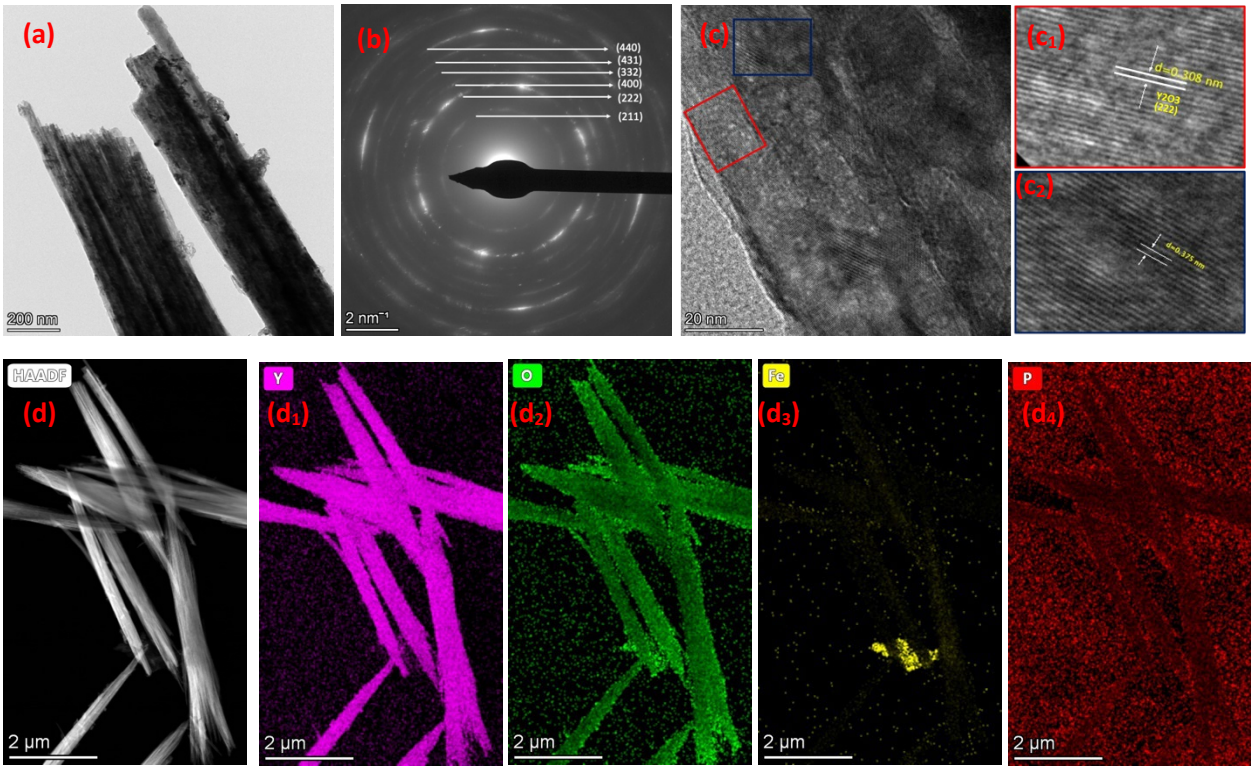

Figure S2: (a) TEM images, (b) SAED pattern, (c) HRTEM images with corresponding lattice fringe pattern, and (d) Elemental mapping analysis of FeYP19.

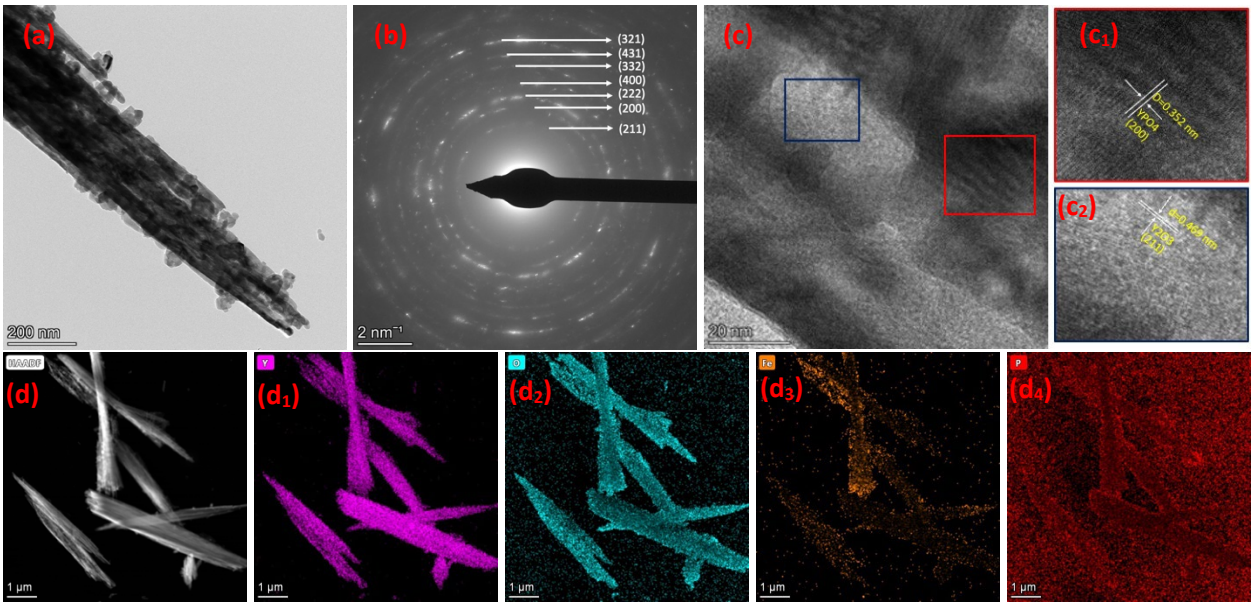

Figure S3: (a) TEM images, (b) SAED pattern, (c) HRTEM images with corresponding lattice fringe pattern, and (d) Elemental mapping analysis of FeYP12.

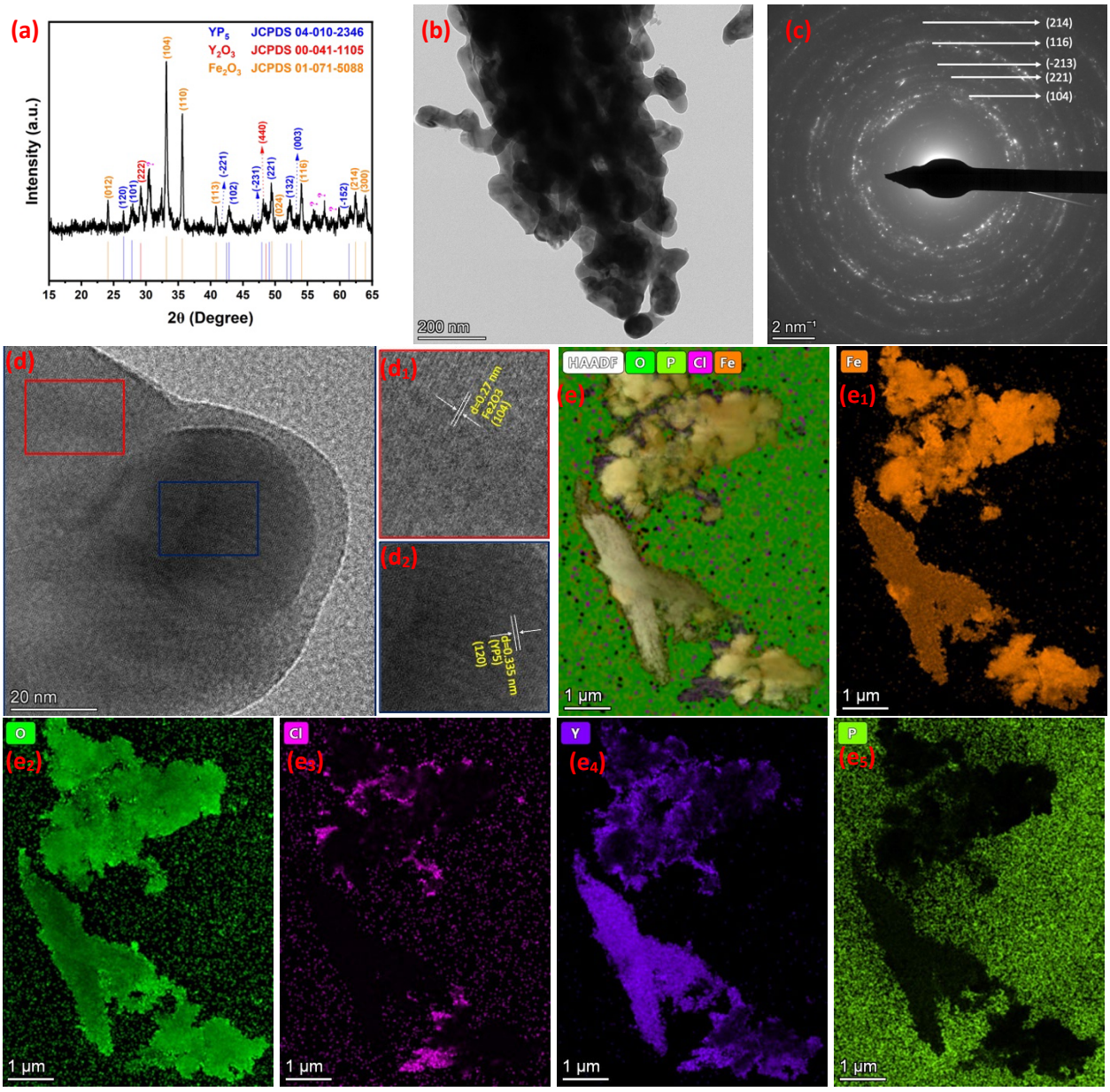

Figure S4: Figure S3: (a) XRD pattern, (b) TEM images, (c) SAED pattern, (d) HRTEM images with corresponding lattice fringe pattern, and (e) Elemental mapping analysis of FeYP21.

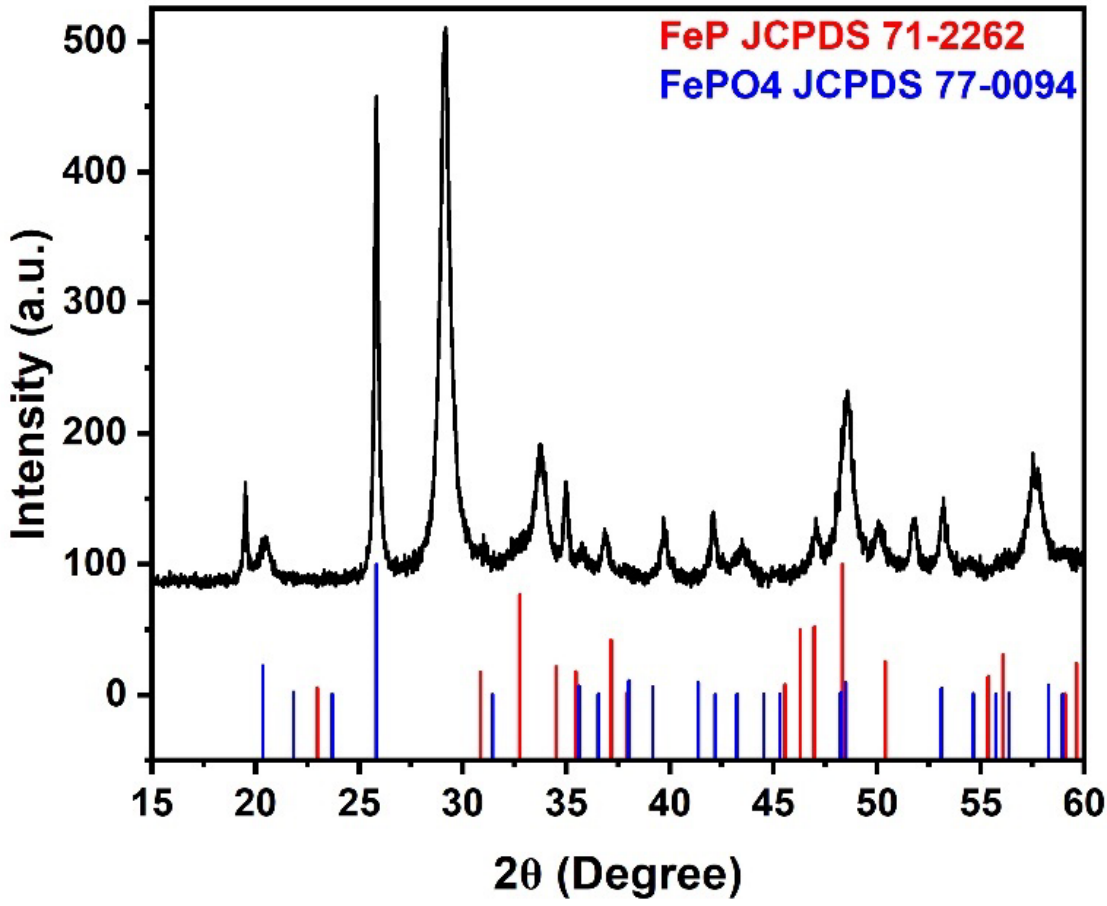

Figure S5: XRD plot of FeYP11 and FeP and FePO4 phase standard card.

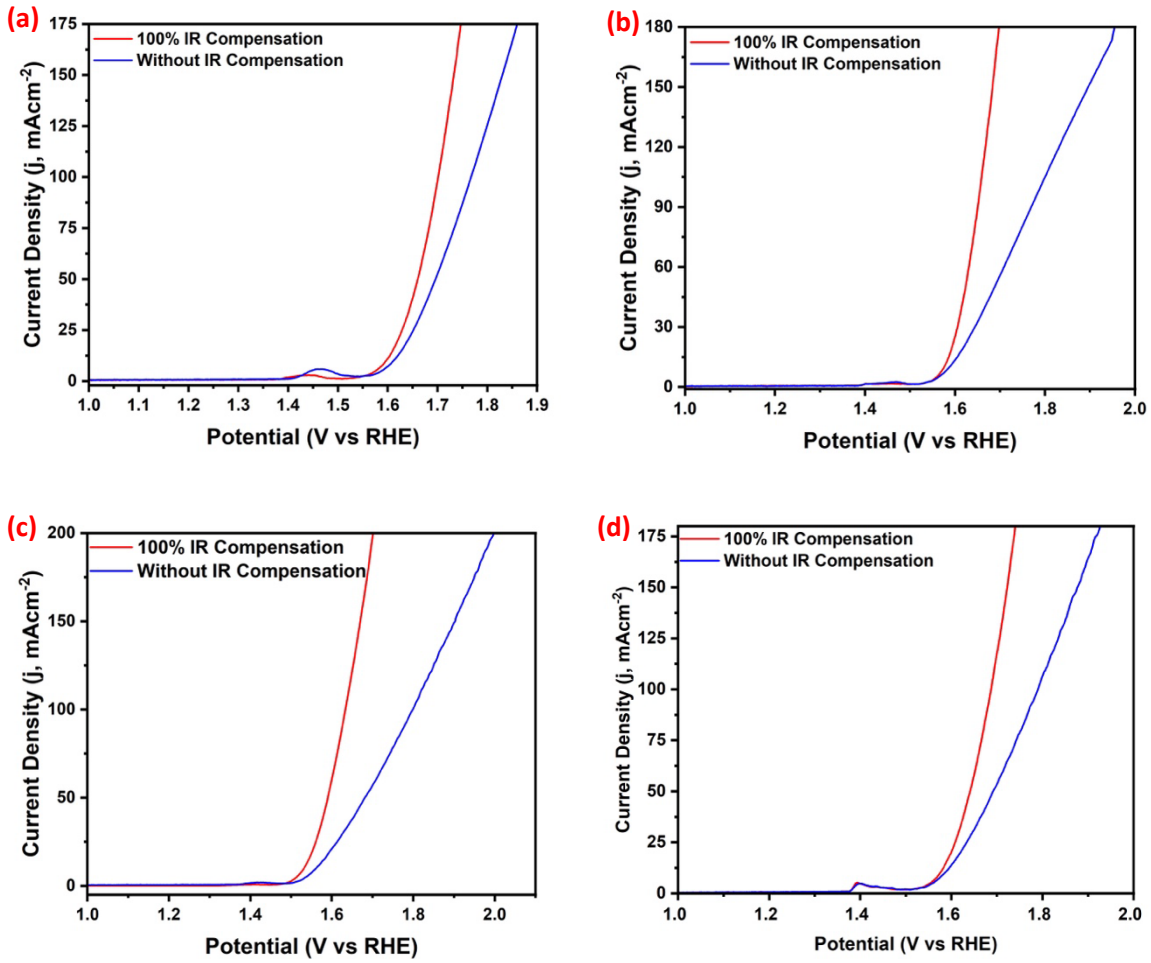

Figure S6: OER LSV plot of a) FeYP19, (b) FeYP12, (c) FeYP11, and (d) FeYP21 with 100% iR compensation and without iR compensation.

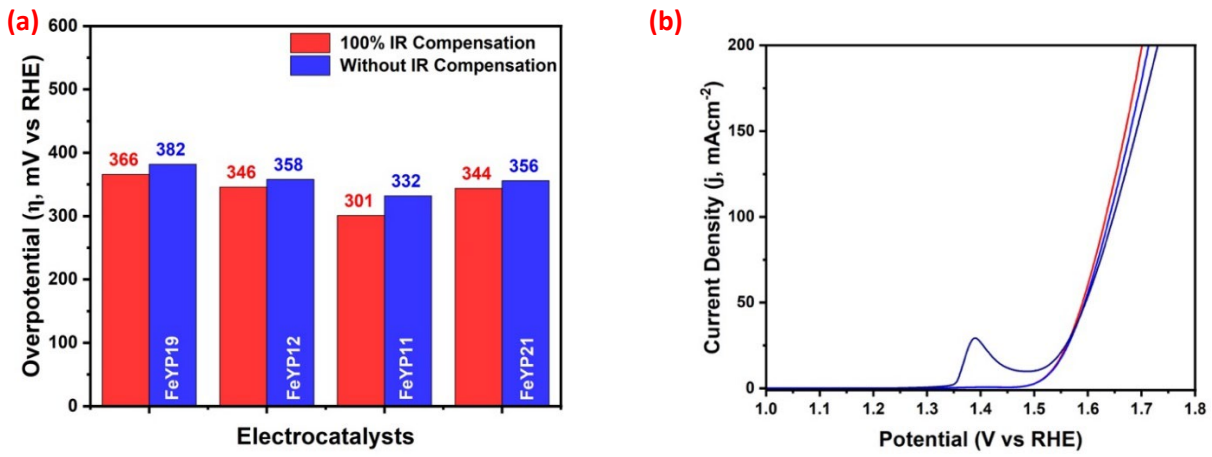

Figure S7: (a) Overpotential for FeYP19, FeYP12, FeYP11, and Fe-YP21 at 10 mVsec-1 with 100%, and without iR compensation, and (b) LSV plot of FeYP11 with 100% iR compensation for reproducibility of OER polarization.

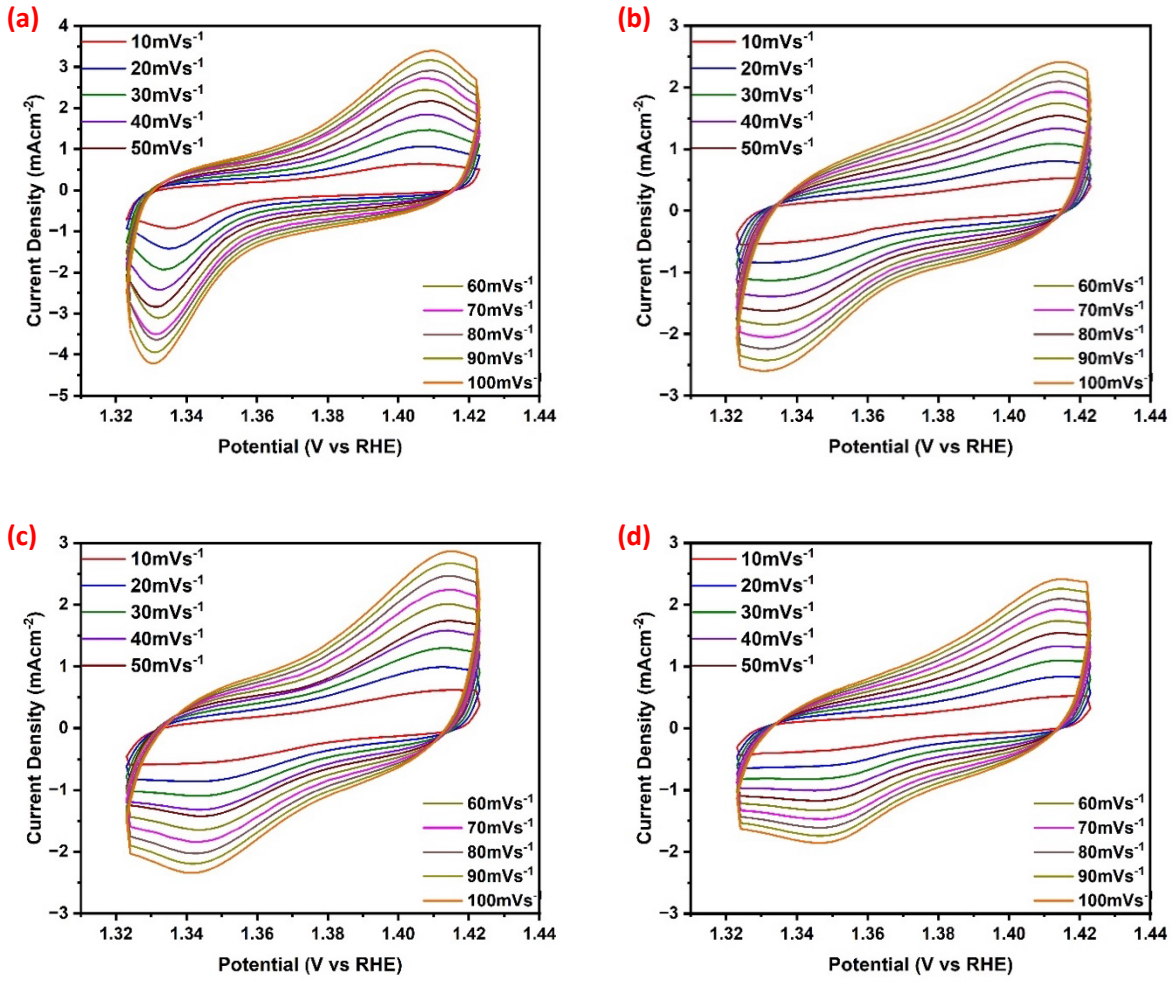

Figure S8: CVs in the non-Faradic region at different scan rates for a) FeYP19, (b) FeYP12, (c) FeYP11, and (d) Fe-YP21 for OER.

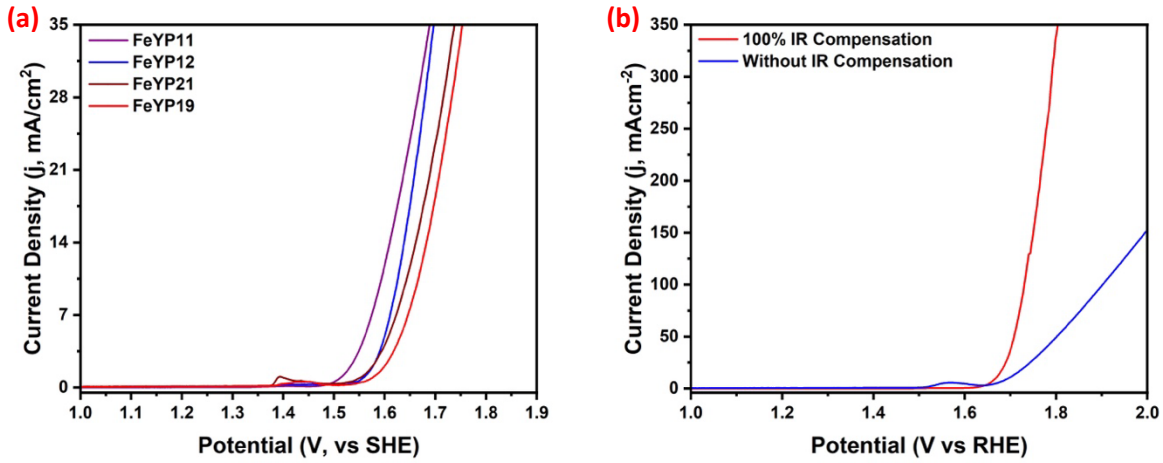

Figure S9: (a) LSV for OER with ECSA normalization, and (b) LSV plot for OER for Fe incorporated yttrium oxide (FeYO11) with 100% and without iR compensation.

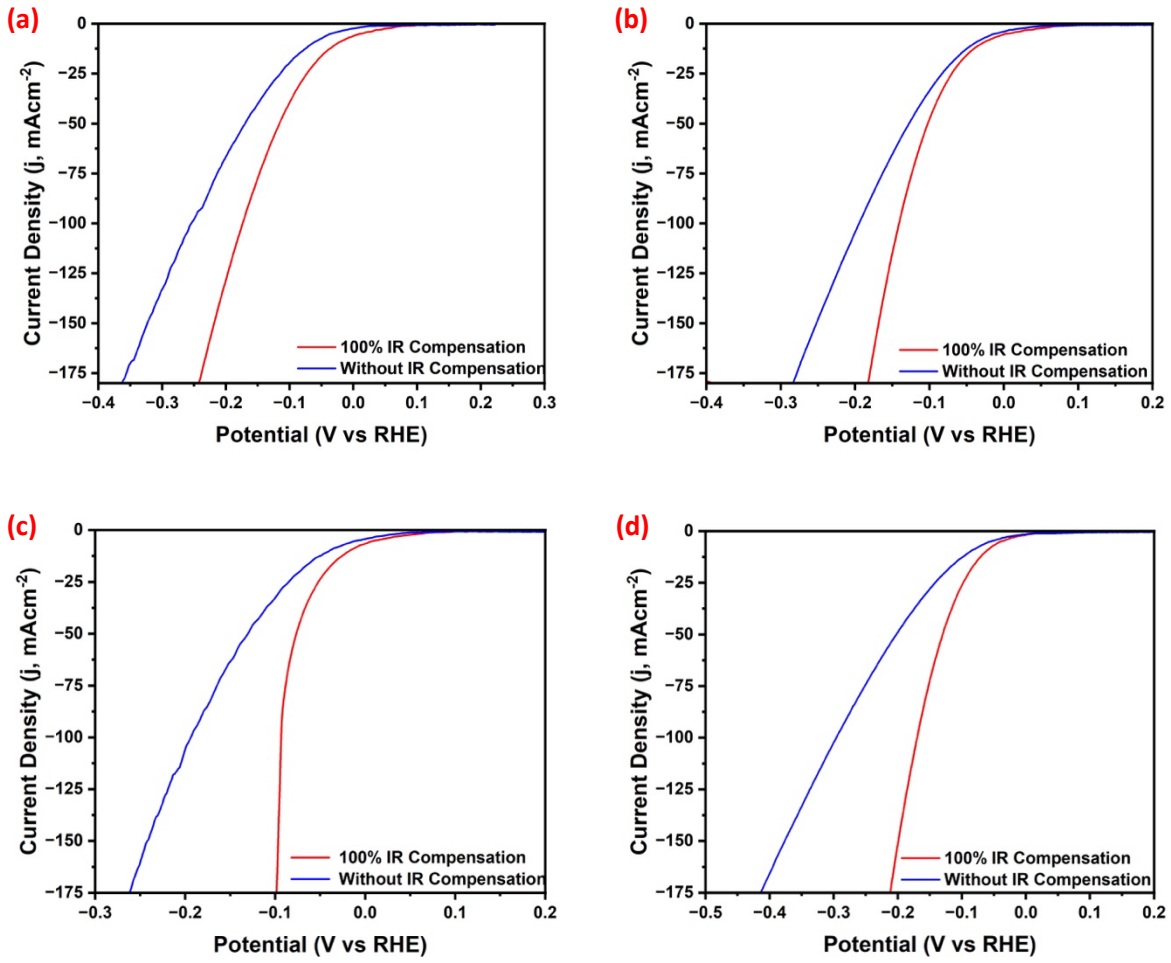

Figure S10: HER LSV plot of a) FeYP19, (b) FeYP12, (c) FeYP11, and (d) FeYP21 with 100% iR compensation and without iR compensation.

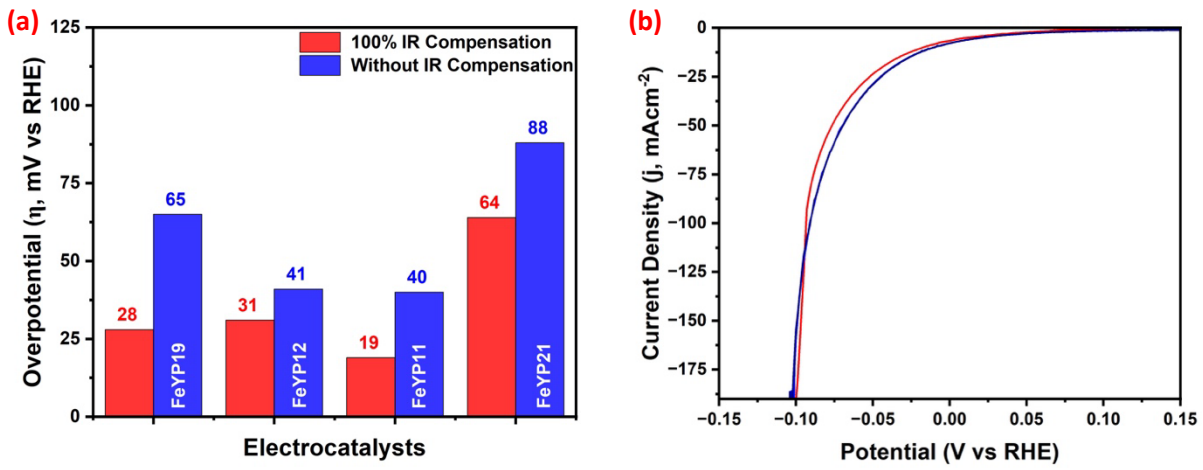

Figure S11: (a) Overpotential for FeYP19, FeYP12, FeYP11, and FeYP21 at 10 $mVsec^{-1}$ with and without iR compensation, and (b) LSV plot of FeYP11 with 100% iR compensation for reproducibility of HER polarization.

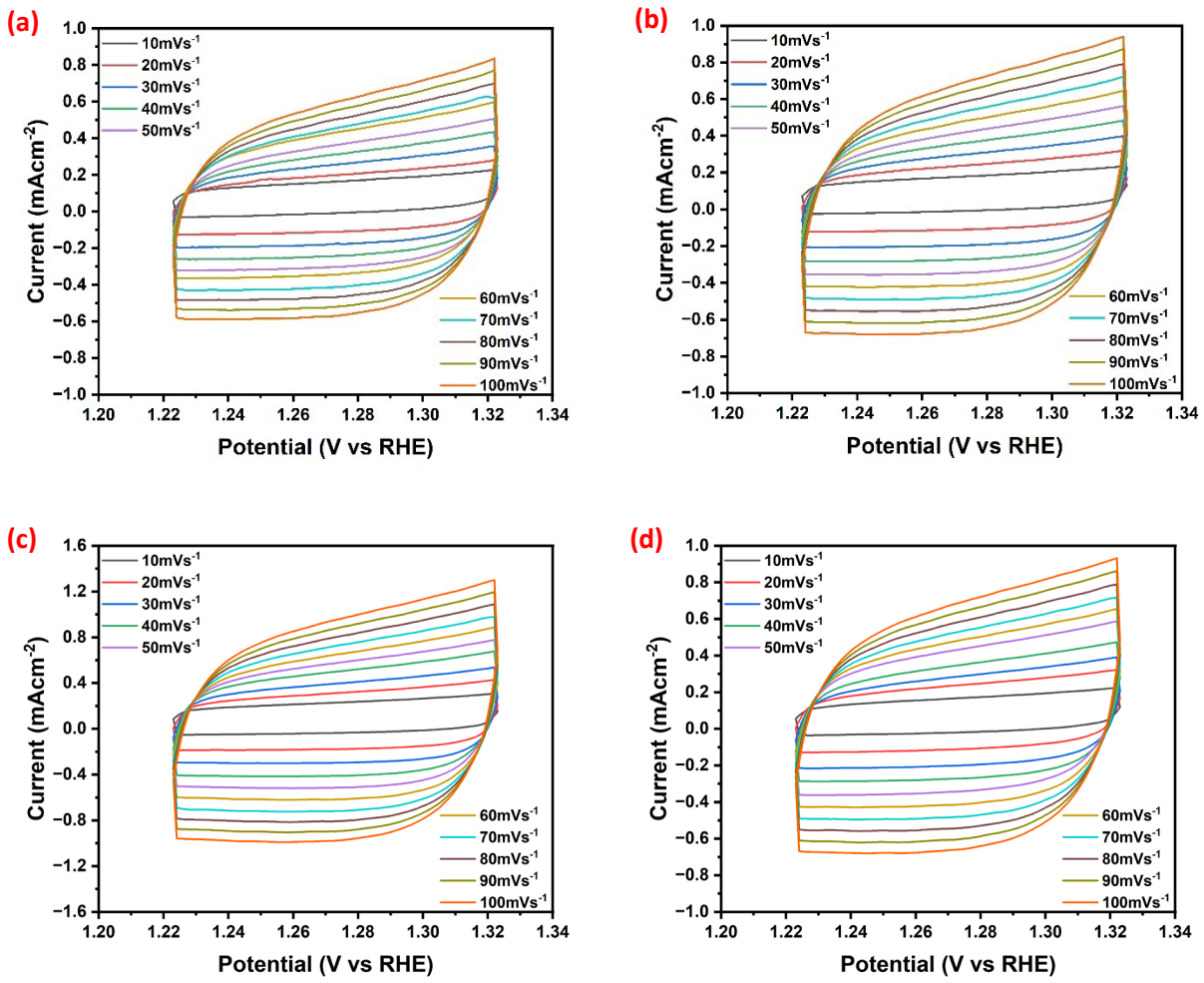

Figure S12: CV in the non-Faradic region at different scan rates for a) FeYP19, (b) FeYP12, (c) FeYP11, and (d) FeYP21 for HER.

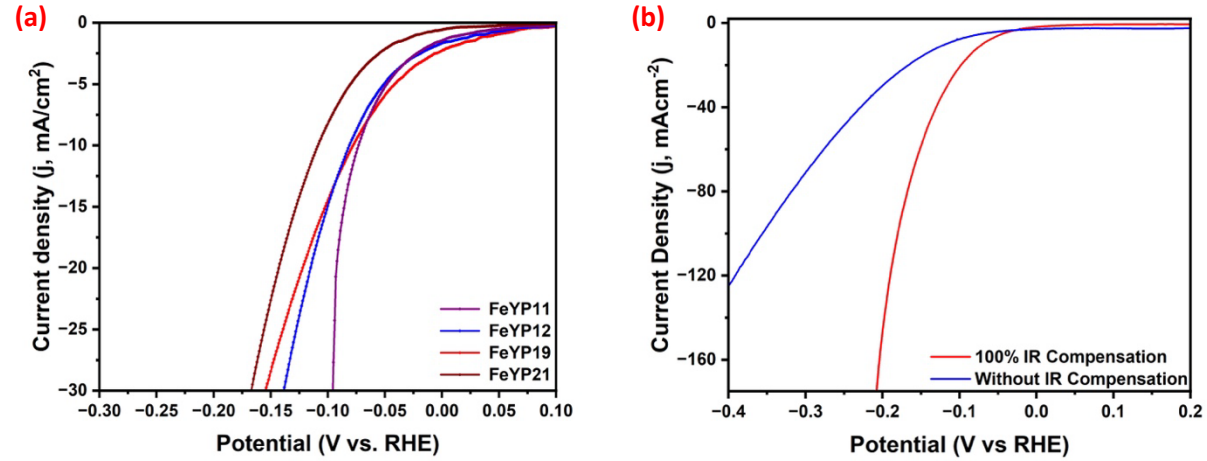

Figure S13: (a) LSV for HER with ESCA normalization, and (b) LSV plot for HER of Fe-incorporated yttrium oxide (FeYO11) with 100% and without iR compensation.

Figure S14: Digital Photograph of (a) the two-electrode symmetric cell electrolyzer, and (b) digital image of the setups for O_2 and H_2 gas collection using a measuring cylinder.

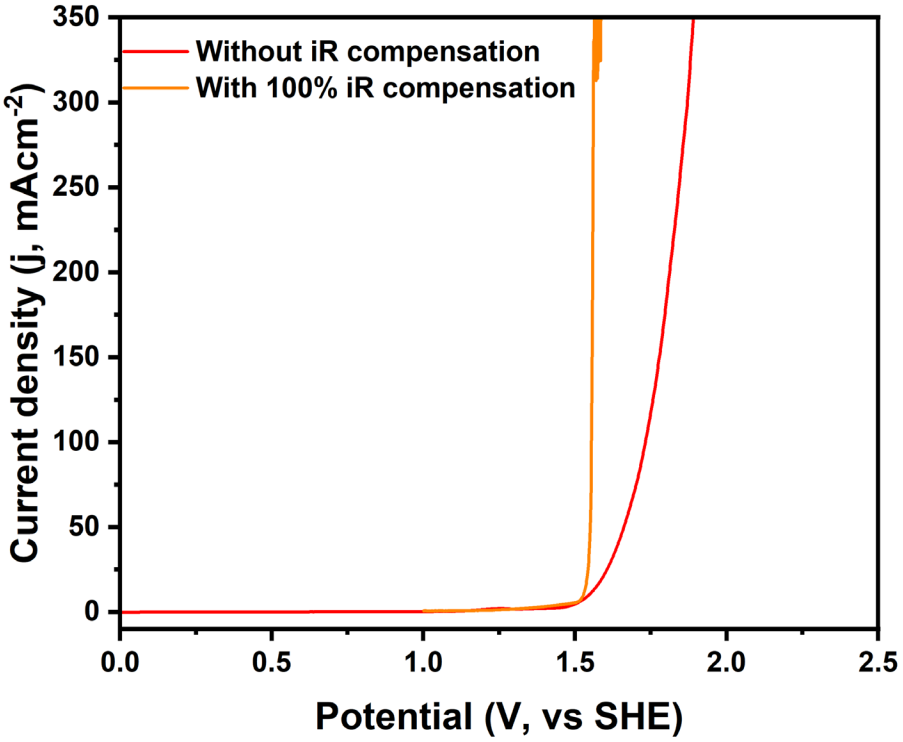

Figure S15: LSV plot of FeYP11 (+) // FeYP11 (-) in a two-electrode system with 100% and without iR compensation.

Table S1: Comparison of overall catalytic performance with previously reported TMPs electrocatalyst.

Catalysts	Substrate	Electrolyte	Overpotential ($10mAcm^{-2}$) (mV)		Cell Voltage	Tafel slope ($mVdec^{-1}$)		Refs.
			η_{HER}	η_{OER}		HER	OER	
FeNiP	NF	1 M KOH	116	235	1.63	68	76	[4]
Ni_2P/Ni_3S_2	NF	1 M KOH	80	210	1.5	65	62	[5]
MoP/Ni_2P	NF	1 M KOH	75	309	1.55	100	78	[6]
$NiSe_2/Ni_2P$	NF	1 M KOH	102	183	1.5	88	45	[7]
FeP/Ni_2P	NF	1M KOH	14	154	1.42	24	23	[8]
Ni_5P_4/NiP_2/NiFe LDH	NF	1 M KOH	124	197	1.52		47	[9]
CoNiP@NiFe LDH	NF	1 M KOH	83	216	1.44	80	45	[10]
NiFe LDH/NiCoP	NF	1 M KOH	120	220	1.57	88	49	[11]
$NiCo_2O_4/Ni_2P$	NF	1 M KOH	45	250	1.59	45	58	[12]
$Ni_2P@FeO_x$	NF	1 M KOH	75	205	1.51		32	[13]
$Ni_2P@NiFeAlO_x$	NF	1 M KOH	105	210	1.52	106	106	[14]
Ni/NiP	NF	1 M KOH	98	200	1.49	72		[15]
FeYP19	NF	1 M KOH	28	113				Our work
FeYP12	NF	1 M KOH	31	106				Our work
FeYP11	NF	1 M KOH	19	67	1.53	66	67	Our work
FeYP21	NF	1 M KOH	64	113				Our work

Supplementary Video: O_2 and H_2 gas collection using a measuring cylinder for faradic efficiency calculation.

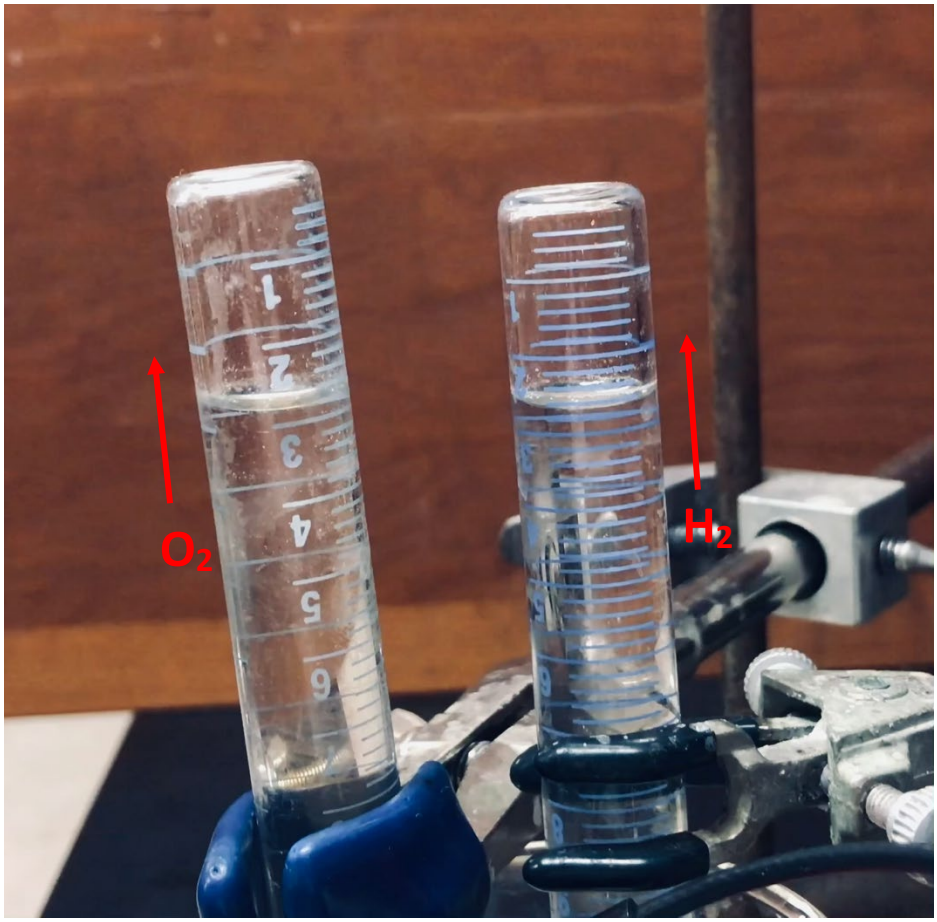

Reference

1. Zheng, W. *iR* Compensation for Electrocatalysis Studies: Considerations and Recommendations. *ACS Energy Lett.* **8**, 1952–1958 (2023).
2. Shinagawa, T., Garcia-Esparza, A. T. & Takanabe, K. Insight on Tafel slopes from a microkinetic analysis of aqueous electrocatalysis for energy conversion. *Sci. Rep.* **5**, 13801 (2015).
3. Xie, X. *et al.* Oxygen Evolution Reaction in Alkaline Environment: Material Challenges and Solutions. *Adv. Funct. Mater.* **32**, 2110036 (2022).
4. Wu, Y. *et al.* Bimetallic Fe-Ni phosphide carved nanoframes toward efficient overall water splitting and potassium-ion storage. *Chem. Eng. J.* **390**, 124515 (2020).
5. Zeng, L. *et al.* Three-dimensional-networked Ni2P/Ni3S2 heteronanoflake arrays for highly enhanced electrochemical overall-water-splitting activity. *Nano Energy* **51**, 26–36 (2018).
6. Du, C., Shang, M., Mao, J. & Song, W. Hierarchical MoP/Ni 2 P heterostructures on nickel foam for efficient water splitting. *J. Mater. Chem. A* **5**, 15940–15949 (2017).
7. Wang, P. *et al.* Coupling NiSe2-Ni2P heterostructure nanowrinkles for highly efficient overall water splitting. *J. Catal.* **377**, 600–608 (2019).
8. Yu, F. *et al.* High-performance bifunctional porous non-noble metal phosphide catalyst for overall water splitting. *Nat. Commun.* **9**, 2551 (2018).
9. Yu, L. *et al.* Amorphous NiFe layered double hydroxide nanosheets decorated on 3D nickel phosphide nanoarrays: a hierarchical core–shell electrocatalyst for efficient oxygen evolution. *J. Mater. Chem. A* **6**, 13619–13623 (2018).
10. Zhou, L. *et al.* Ultrathin CoNiP@Layered Double Hydroxides Core–Shell Nanosheets Arrays for Largely Enhanced Overall Water Splitting. *ACS Appl. Energy Mater.* **1**, 623–631 (2018).

11. Zhang, H. *et al.* Bifunctional Heterostructure Assembly of NiFe LDH Nanosheets on NiCoP Nanowires for Highly Efficient and Stable Overall Water Splitting. *Adv. Funct. Mater.* **28**, 1706847 (2018).
12. Wang, Q. *et al.* NiCo2O4@Ni2P nanorods grown on nickel nanorod arrays as a bifunctional catalyst for efficient overall water splitting. *Mater. Today Energy* **17**, 100490 (2020).
13. Zhang, F.-S. *et al.* Extraction of nickel from NiFe-LDH into Ni 2 P@NiFe hydroxide as a bifunctional electrocatalyst for efficient overall water splitting. *Chem. Sci.* **9**, 1375–1384 (2018).
14. Gao, Z., Liu, F., Wang, L. & Luo, F. Hierarchical Ni2P@NiFeAlOx Nanosheet Arrays as Bifunctional Catalysts for Superior Overall Water Splitting. *Inorg. Chem.* **58**, 3247–3255 (2019).
15. You, B., Jiang, N., Sheng, M., Bhushan, M. W. & Sun, Y. Hierarchically Porous Urchin-Like Ni2P Superstructures Supported on Nickel Foam as Efficient Bifunctional Electrocatalysts for Overall Water Splitting. *ACS Catal.* **6**, 714–721 (2016).